Frontiers in Bioscience Landmark

Front. Biosci. (Landmark Ed) **2026**; 31(1): 47910
https://doi.org/10.31083/FBL47910

Original Research

Oncogenic Role of *KIF18B* Across Human Cancers: A Pan-Cancer Bioinformatic Analysis and Experimental Validation in Lung Adenocarcinoma

Junli Hou[1,†], Xiangrong Shao[1,†], Yawen Zhang[1], Feng Jin[1], Wenwen Xu[1], Xiantao Xu[1,*]

[1]Department of Respiratory and Critical Care Medicine, The Affiliated Hospital of Yangzhou University, Yangzhou University, 225000 Yangzhou, Jiangsu, China

*Correspondence: xuxt3805@163.com (Xiantao Xu)

[†]These authors contributed equally.

Academic Editor: Amancio Carnero Moya

Submitted: 2 November 2025 Revised: 19 December 2025 Accepted: 31 December 2025 Published: 21 January 2026

Abstract

Background: Identifying oncogenic drivers with broad relevance across multiple cancer types is critical for developing novel therapeutic strategies. Kinesin family member 18B (*KIF18B*) is involved in mitotic regulation, but its comprehensive role and clinical significance across human malignancies remain poorly understood. This study performed a comprehensive pan-cancer analysis of *KIF18B* and experimentally validated its role in lung adenocarcinoma (LUAD). **Methods**: We conducted a comprehensive bioinformatic analysis using public databases to evaluate the expression profile, prognostic value, and potential biological functions of *KIF18B* across various human cancers. Based on these findings, LUAD was selected for further investigation. We evaluated KIF18B protein levels in LUAD cell lines (A549, HCC827, H1975) and compared them to a normal bronchial epithelial cell line (BEAS-2B). Subsequently, KIF18B was silenced in A549 cells using small interfering RNA (siRNA), and its effects on cell proliferation, migration, and invasion were examined using colony formation, wound-healing, and Transwell assays. **Results**: Our analysis across various cancers revealed that *KIF18B* is markedly overexpressed, including in LUAD, and this high expression correlates with poor prognosis in patients across different cancer types. In line with these bioinformatic results, our experiments confirmed that KIF18B protein levels were elevated in LUAD cell lines compared with normal controls. Functional assays demonstrated that knockdown of KIF18B in A549 cells significantly suppressed colony-forming ability and impaired migratory and invasive capacities. **Conclusions**: This study, integrating pan-cancer bioinformatic analysis with experimental validation, establishes *KIF18B* as a widely expressed oncogene with significant prognostic value. Our findings in LUAD confirm its crucial role in promoting key malignant phenotypes. Thus, *KIF18B* emerges as a valuable prognostic biomarker and a potential therapeutic target, not only for LUAD but potentially for a wider array of cancers.

Keywords: kinesins; adenocarcinoma of lung; prognosis; biomarkers; oncogenes

1. Introduction

Lung cancer is a major contributor to cancer-related morbidity and mortality worldwide, significantly impacting global public health [1,2]. Lung adenocarcinoma (LUAD), the most common form of non-small cell lung cancer (NSCLC), is marked by its complex pathogenesis and significant heterogeneity [3–5]. Despite advancements in targeted therapies and immunotherapies, the 5-year survival rate for LUAD remains low due to drug resistance and tumor recurrence [6–8]. This highlights the urgent need to explore the molecular mechanisms driving LUAD progression and to discover new prognostic biomarkers and therapeutic targets to enhance clinical outcomes.

The Kinesin Superfamily Proteins (KIFs) are crucial ATP-dependent motor proteins involved in vital cellular functions, including mitosis, intracellular transport, and maintaining cell morphology by traversing microtubule tracks [9–11]. *KIF18B*, a member of the kinesin-8 subfamily, classically functions as a microtubule depolymerase to precisely regulate chromosome alignment during metaphase, thereby ensuring genomic stability [12,13]. Emerging evidence has implicated the aberrant expression of various KIFs in malignant progression, acting as potential oncogenes or tumor suppressors [14,15]. However, a comprehensive landscape of *KIF18B* and its clinical significance remain largely uncharacterized. Its expression profile across diverse cancer types, its general association with patient prognosis, and its specific biological functions, particularly in a high-incidence malignancy like LUAD, have not been systematically investigated or experimentally validated.

This study aims to fill this knowledge gap by exploring the role of *KIF18B* across various cancers, with a focus on LUAD. By investigating its expression profile and prognostic relevance, we hope to establish *KIF18B* as a potential oncogene and highlight its promise as a prognostic biomarker and therapeutic target in LUAD.

2. Materials and Methods

2.1 Pan-Cancer Expression Landscape of KIF18B

To comprehensively characterize the expression profile of *KIF18B* across various human malignancies, we systematically investigated its transcriptional landscape using publicly available datasets. We obtained RNA sequencing data (HTSeq-FPKM format) and clinical annotations for 33 cancer types from The Cancer Genome Atlas (TCGA) via the UCSC Xena platform. To ensure reliable comparisons across samples and genes, all FPKM expression values were converted to Transcripts Per Million (TPM). For subsequent statistical analyses and visualizations, these TPM values underwent a log2(TPM + 1) transformation.

2.2 Differential Expression Analysis of KIF18B

Differential expression of *KIF18B* between tumor tissues and their corresponding normal counterparts was evaluated using the Wilcoxon Rank Sum Test. The results were presented as boxplots to clearly display the expression distribution across different cancer types. To broaden the comparison against a baseline of healthy tissues, we integrated data from the Genotype-Tissue Expression (GTEx) project, allowing for a comparison of *KIF18B* expression in TCGA primary tumors against a wide array of normal tissues.

2.3 Evaluation of KIF18B's Diagnostic Potential

To determine the diagnostic utility of *KIF18B* expression for distinguishing between malignant and non-malignant tissues, we employed Receiver Operating Characteristic (ROC) analysis. For each cancer type, the pROC package in R was used to calculate the Area Under the Curve (AUC) and its 95% confidence interval. In our study, an AUC value above 0.7 was considered indicative of acceptable diagnostic accuracy, while values above 0.9 were interpreted as excellent diagnostic accuracy. The smoothed ROC curves were used to visually illustrate *KIF18B*'s diagnostic potential, with particular emphasis on cancer types where the AUC exceeded 0.9, signifying robust discriminatory power.

2.4 Prognostic Significance of KIF18B

To comprehensively investigate the prognostic value of *KIF18B*, we assessed its association with Overall Survival (OS). For each cancer type and survival metric, patients were dichotomized into high- and low- *KIF18B* expression cohorts. The optimal expression threshold for this stratification was determined via the surv_cutpoint function within the survminer R package (version 3.5-5; CRAN, https://cran.r-project.org/). To ensure the analytical robustness and prevent bias arising from highly imbalanced groups, a minimum patient ratio of 0.3 between the high- and low-expression cohorts was strictly maintained. Kaplan-Meier curves were created to visually represent survival differences, with statistical significance between the survival curves of the two groups assessed using the log-rank test via the survfit function. All survival analyses were performed in R, leveraging the functionalities of the survival and survminer packages.

2.5 Characterization of the KIF18B-Associated Immune Landscape

To characterize the immunological context of *KIF18B*, we drew upon the extensive data from "The Immune Landscape of Cancer" study, which provides immunogenomic profiles for over 10,000 TCGA tumors across 33 cancer types [16]. Our analysis proceeded in two parts. First, we explored the co-expression patterns between *KIF18B* and a panel of immune-related genes within each malignancy. Pearson correlation coefficients were computed, and the results were displayed as heatmaps using the ComplexHeatmap package (version 1.18.1; Bioconductor, https://bioconductor.org/packages/ComplexHeatmap/). In these visualizations, red and blue color gradients represent the strength of positive and negative correlations, respectively.

We explored the relationship between *KIF18B* expression and six recognized cancer immune subtypes. Patients were divided into high- and low-*KIF18B* expression groups based on the median expression value. We compared the distribution of these immune subtypes between the groups and used a chi-square test to evaluate the statistical significance of any associations. These dual analyses provide a comprehensive view of *KIF18B*'s relationship with the tumor immune environment, offering insights that could be pivotal for developing more personalized and effective immunotherapies [16].

2.6 Functional Role and Pathway Analysis of KIF18B

To delineate the functional role of *KIF18B*, we first examined its association with 14 distinct cancer functional states cataloged in the CancerSEA database [17]. Gene set scores representing the activity of these states were standardized using the scale function, and their Pearson correlations with *KIF18B* expression were calculated.

We then explored the impact of *KIF18B* on the broader transcriptome. Tumors were stratified into *KIF18B*-high (top 30% expression) and *KIF18B*-low (bottom 30% expression) cohorts. Next, we conducted differential expression analysis with the limma package to identify genes significantly different between the two groups, ranking them by log2 fold change (log2FC) ($|\text{log2FC}| \geq 1$ was used as the screening criterion). Furthermore, we investigated *KIF18B*'s relationship with the tumor microenvironment and genome integrity. We used Spearman's correlation to quantify the relationship between *KIF18B* expression and the abundance of various immune infiltrating cells, presenting the findings in a heatmap.

Simultaneously, we utilized heatmaps to visualize correlations between *KIF18B* expression and selected functional proteins from the TCGA cancer database. Significant positive correlations are highlighted in red, significant

negative correlations in blue, and non-significant correlations in white. The intensity of the colors is proportional to the absolute value of the correlation coefficient. Additionally, we examined correlations between *KIF18B* expression and key genomic features such as aneuploidy, homologous recombination defects, tumor ploidy, SNV neoantigens, silent mutation rate, and nonsilent mutation rate using the cor.test function [18]. These genomic correlations were summarized across cancer types in a radar chart created with the fmsb package (version 0.7.6; CRAN, https://cran.r-project.org/web/packages/fmsb/index.html).

2.7 Differential Expression and Prognostic Value of KIF18B in LUAD

We began our analysis by examining *KIF18B* expression differences in Lung Adenocarcinoma (LUAD). Using the Wilcoxon Rank Sum Test, we compared *KIF18B* levels in tumor tissues versus adjacent normal tissues within the TCGA-LUAD cohort. We also explored the relationship between *KIF18B* expression and tumor grade. To validate these expression patterns, we performed an external analysis on three independent datasets from the Gene Expression Omnibus (GEO): GSE19188 (Samples: 156, Platform: GPL570), GSE13213 (Samples: 117, Platform: GPL6480), and GSE72094 (Samples: 442, Platform: GPL15048).

To assess its prognostic value, we performed a survival analysis on LUAD data, dividing patients into high- and low-*KIF18B* expression groups. The Kaplan-Meier survival curves for these groups were compared using a log-rank test, implemented with the survfit function from the R 'survival' package (version 3.5-5; CRAN, https://cran.r-project.org/), to evaluate the statistical significance of survival differences.

2.8 RNA Isolation and Reverse Transcription-Quantitative Polymerase Chain Reaction (RT-qPCR)

To experimentally validate *KIF18B* expression at the mRNA level, RT-qPCR was performed on Lung Adenocarcinoma (LUAD) and adjacent non-tumorous tissues. Tissue samples were obtained from patients who underwent surgical resection at The Affiliated Hospital of Yangzhou University, Yangzhou University. This study was conducted in compliance with the Declaration of Helsinki and received ethical approval from the Institutional Review Board of The Affiliated Hospital of Yangzhou University (Approval Number: 2024-YKL07-SW007). Informed consent was obtained from all participating patients. Total RNA was isolated from tissue samples using a standard RNA extraction kit (catalog no. R2050, Zymo Research, Irvine, CA, USA), followed by reverse transcription into cDNA using a synthesis kit (catalog no. K1622, Thermo Scientific, China). The quantitative PCR amplification was then carried out using specific primers for *KIF18B* (Forward: 5′-GGTGTGGGTACTGCTGTCTG-3′, Reverse: 5′-ACTGTGGTGACACCTTTCGT-3′) and the internal control, GAPDH. This study was conducted in compliance with the Declaration of Helsinki and received ethical approval from the Institutional Review Board of The Affiliated Hospital of Yangzhou University (Approval Number: 2024-YKL07-SW007).

2.9 Western Blot Analysis

For protein expression analysis, we conducted Western blotting on protein lysates from LUAD samples. Tissue samples were sourced from The Affiliated Hospital of Yangzhou University, Yangzhou University, with informed consent obtained from all patients. Protein concentrations were measured with a BCA protein assay kit (catalog no. PC0020, Solarbio, Beijing, China). Equal amounts of protein were mixed with loading buffer, denatured, and separated on 15% SDS-PAGE gels. Proteins were then transferred to 0.22-µm polyvinylidene fluoride (PVDF) membranes. After blocking with 5% bovine serum albumin (BSA), membranes were incubated overnight at 4 °C with primary antibodies against KIF18B (1:200, catalog no. ab121798, Abcam, Cambridge, UK) and GAPDH (1:5000, catalog no. 10494-1-AP, Proteintech, Rosemont, IL, USA). The membranes were then incubated with corresponding fluorescent secondary antibodies. Protein bands were visualized using the Odyssey infrared imaging system (Model 9120; LI-COR Biosciences, Lincoln, NE, USA), and their densities were quantified for analysis.

2.10 Cell Culture

Human lung adenocarcinoma cell lines (A549, HCC827, H1975) and a human bronchial epithelial cell line (BEAS-2B, used as a control) were obtained from the Cell Bank of the Chinese Academy of Sciences (Shanghai, China). All media were supplemented with 10% Fetal Bovine Serum (FBS; catalog no. SH30070.03, HyClone, Logan, UT, USA) and 1% penicillin/streptomycin (catalog no. 15140122, Invitrogen, Carlsbad, CA, USA). Cells were maintained in a humidified incubator at 37 °C with 5% CO_2. Mycoplasma contamination was routinely monitored using a detection kit (LT07-418, Lonza, Basel, Switzerland) to ensure cell culture purity. All cell lines were validated by short tandem repeat (STR) profiling and tested negative for mycoplasma.

2.11 Small Interfering RNA (siRNA) Transfection

Based on our initial Western blot screening, which showed the highest endogenous KIF18B protein expression in the A549 cell line among the tested cancer cells, A549 was selected for subsequent gene knockdown experiments. Additionally, knockout efficiency was also validated in the H1975 cell line. Three distinct small interfering RNAs targeting *KIF18B* (si-KIF18B#1, si-KIF18B#2, si-KIF18B#3) and a negative control siRNA (si-NC) were synthesized by Invitrogen (catalog no.1299003, Carlsbad, CA, USA). For transient transfection, A549 and H1975 cells were seeded

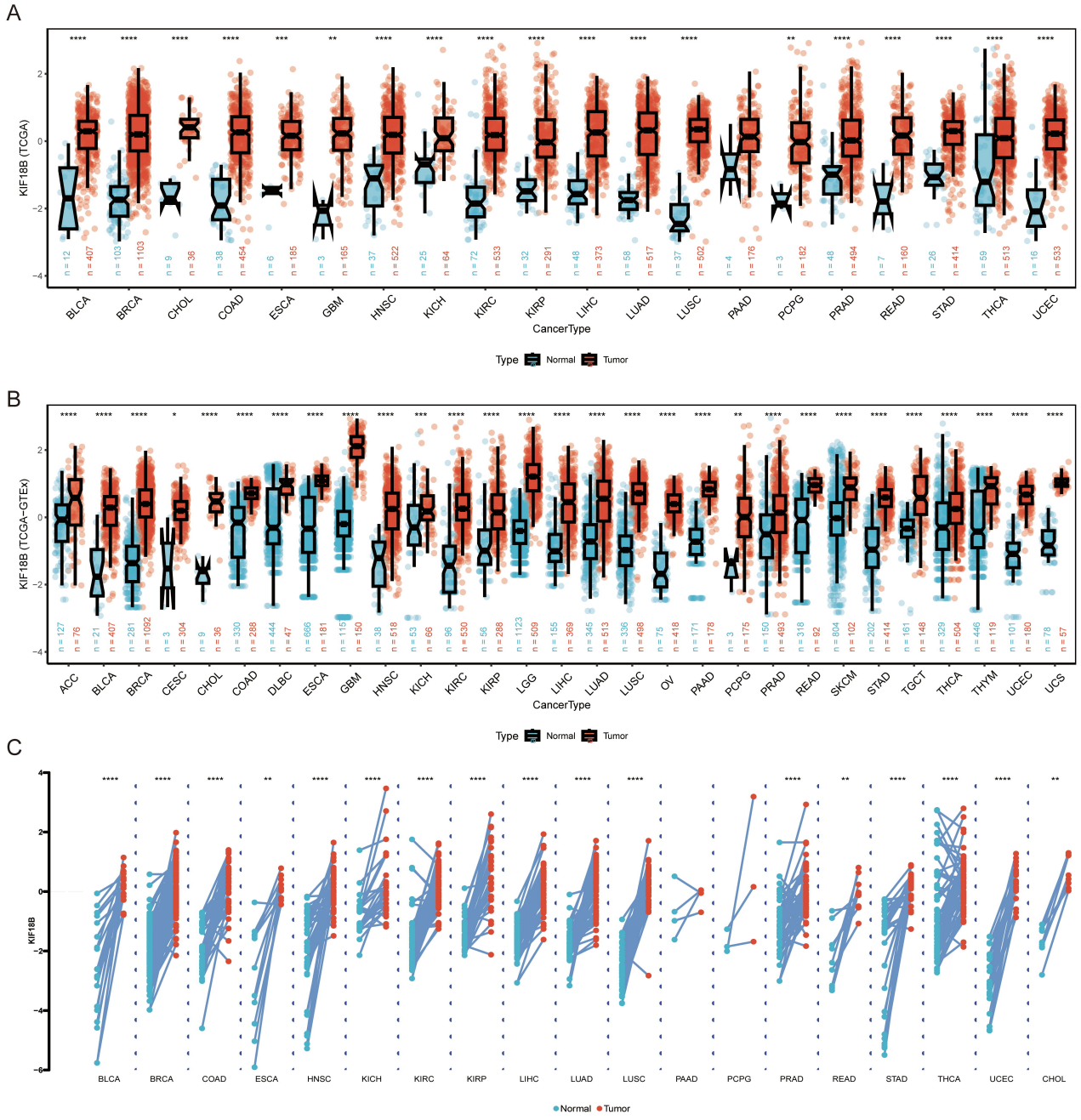

Fig. 1. Pan-cancer analysis reveals widespread overexpression of *Kinesin Family Member 18B* (*KIF18B*). (A) Differential expression of *KIF18B* between tumor tissues from The Cancer Genome Atlas (TCGA) and their corresponding adjacent normal tissues. (B) Differential expression of *KIF18B* in tumor samples (TCGA) compared to normal tissues from the Genotype-Tissue Expression (GTEx) database. (C) Paired analysis showing KIF18B transcript levels in tumor versus adjacent normal tissues across various TCGA cancer types. *$p < 0.05$, **$p < 0.01$, ***$p < 0.001$, ****$p < 0.0001$.

into 6-well plates and transfected with siRNAs using Lipofectamine 3000 Reagent (catalog no. L3000008, Invitrogen, Carlsbad, CA, USA) following the manufacturer's instructions. Cells were collected for further analysis 48 hours after transfection.

2.12 Colony Formation Assay

To assess the impact of KIF18B knockdown on long-term cell growth and survival, we conducted a colony formation assay. A549 cells transfected with si-KIF18B or si-NC were seeded into 6-well plates. After incubation, colonies were washed with PBS, fixed with 4% paraformaldehyde for 30 minutes, and stained with 0.1%

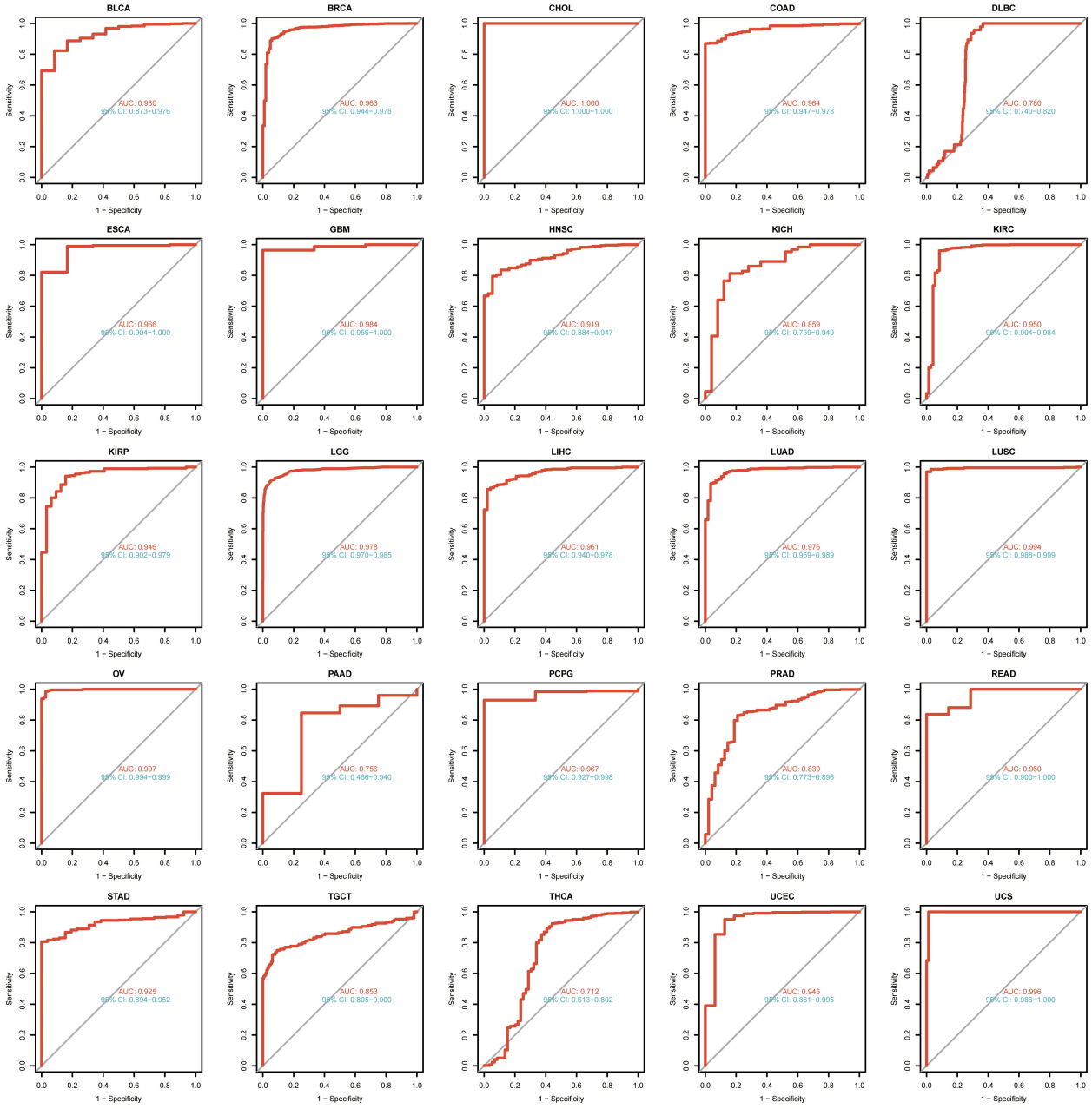

Fig. 2. Diagnostic value of *KIF18B* expression in distinguishing tumor from normal tissues. Receiver Operating Characteristic (ROC) curve analysis assessing the diagnostic efficacy of *KIF18B* expression. The curves illustrate the ability of *KIF18B* to differentiate tumor from normal tissues across multiple cancer types. BLCA, Bladder Urothelial Carcinoma; BRCA, Breast Invasive Carcinoma; DLBC, Lymphoid Neoplasm Diffuse Large B-cell Lymphoma; ESCA, Esophageal Carcinoma; GBM, Glioblastoma Multiforme; HNSC, Head and Neck Squamous Cell Carcinoma; KICH, Kidney Chromophobe; KIRC, Kidney Renal Clear Cell Carcinoma; KIRP, Kidney Renal Papillary Cell Carcinoma; LAML, Acute Myeloid Leukemia; LGG, Brain Lower Grade Glioma; LIHC, Liver Hepatocellular Carcinoma; LUAD, Lung Adenocarcinoma; LUSC, Lung Squamous Cell Carcinoma; OV, Ovarian Serous Cystadenocarcinoma; PAAD, Pancreatic Adenocarcinoma; PCPG, Pheochromocytoma and Paraganglioma; PRAD, Prostate Adenocarcinoma; READ, Rectum Adenocarcinoma; STAD, Stomach Adenocarcinoma; TGCT, Testicular Germ Cell Tumors; THCA, Thyroid Carcinoma; UCEC, Uterine Corpus Endometrial Carcinoma; UCS, Uterine Carcinosarcoma.

crystal violet for 30 minutes. After washing and air-drying, the plates were photographed. Each experiment was conducted in triplicate.

2.13 Wound Healing Assay

The wound healing assay was used to evaluate the migratory capacity of A549 cells. Transfected cells were

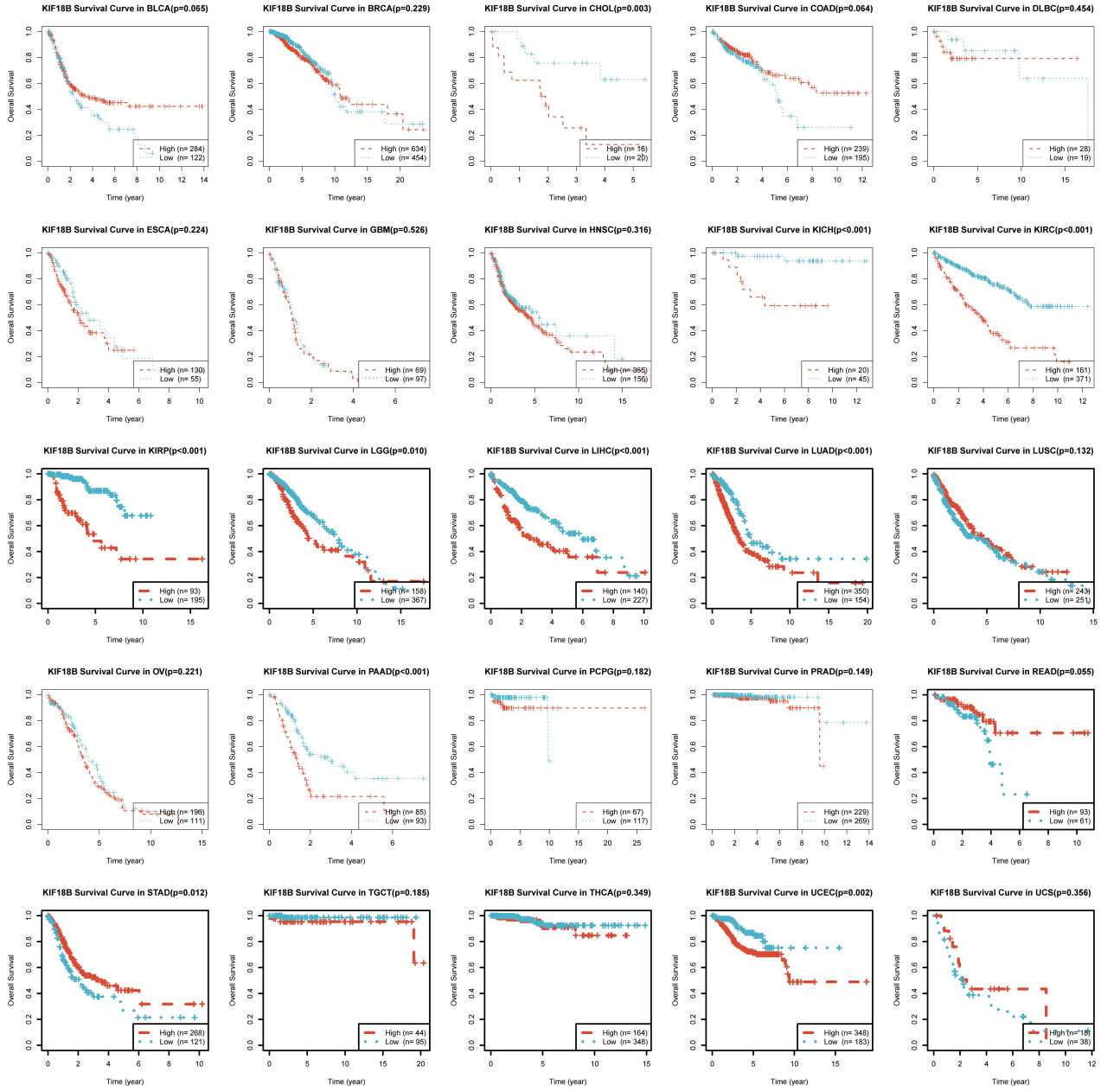

Fig. 3. Dual prognostic role of *KIF18B* across different cancer types. Kaplan-Meier survival curves illustrating the association between *KIF18B* expression and Overall Survival (OS) in cancer patients. High level *KIF18B* expression is correlated with poor prognosis in malignancies such as LUAD, KIRC, and LIHC, while it is associated with a favorable prognosis in others, including STAD (log-rank $p < 0.05$). BLCA, Bladder Urothelial Carcinoma; BRCA, Breast Invasive Carcinoma; DLBC, Lymphoid Neoplasm Diffuse Large B-cell Lymphoma; ESCA, Esophageal Carcinoma; GBM, Glioblastoma Multiforme; HNSC, Head and Neck Squamous Cell Carcinoma; KICH, Kidney Chromophobe; KIRC, Kidney Renal Clear Cell Carcinoma; KIRP, Kidney Renal Papillary Cell Carcinoma; LAML, Acute Myeloid Leukemia; LGG, Brain Lower Grade Glioma; LIHC, Liver Hepatocellular Carcinoma; LUAD, Lung Adenocarcinoma; LUSC, Lung Squamous Cell Carcinoma; OV, Ovarian Serous Cystadenocarcinoma; PAAD, Pancreatic Adenocarcinoma; PCPG, Pheochromocytoma and Paraganglioma; PRAD, Prostate Adenocarcinoma; READ, Rectum Adenocarcinoma; STAD, Stomach Adenocarcinoma; TGCT, Testicular Germ Cell Tumors; THCA, Thyroid Carcinoma; UCEC, Uterine Corpus Endometrial Carcinoma; UCS, Uterine Carcinosarcoma.

grown in 6-well plates until reaching 90–100% confluence. A sterile 200 µL pipette tip was used to make a straight scratch in the cell monolayer. Images of the scratch were taken at 0 and 36 hours using an inverted microscope

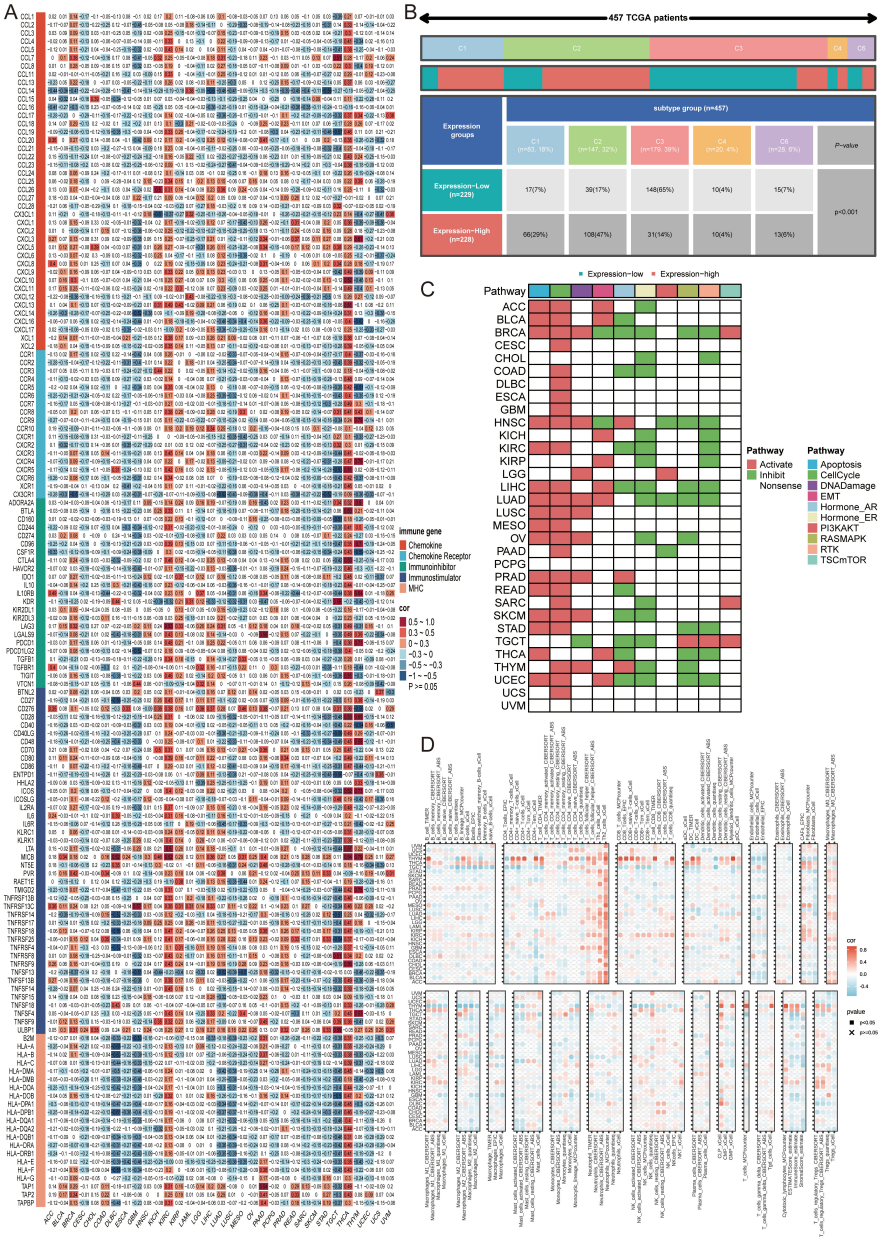

Fig. 4. Association of *KIF18B* expression with the tumor immune microenvironment and cancer-related pathways. (A) Heatmap displaying the co-expression patterns of *KIF18B* and a panel of pro-inflammatory and immune-suppressive genes across various cancers. (B) Distribution of immune subtypes (C1–C6) in high- and low-*KIF18B* expression groups, showing a significant divergence (chi-square test, $p < 0.001$). (C) Box plots representing the differential activity of key cancer-related pathways (Epithelial-Mesenchymal Transition, Cell Cycle, DNA Damage Response) between high- and low-*KIF18B* cohorts (Wilcoxon test, $p < 0.05$). (D) A heatmap was created to visualize the relationship between KIF18B expression and the infiltration levels of different immune cell populations across various cancer types. ACC, Adrenocortical Carcinoma; BLCA, Bladder Urothelial Carcinoma; BRCA, Breast Invasive Carcinoma; CESC, Cervical Squamous Cell Carcinoma and Endocervical Adenocarcinoma; CHOL, Cholangiocarcinoma; COAD, Colon Adenocarcinoma; DLBC, Lymphoid Neoplasm Diffuse Large B-cell Lymphoma; ESCA, Esophageal Carcinoma; GBM, Glioblastoma Multiforme; HNSC, Head and Neck Squamous Cell Carcinoma; KICH, Kidney Chromophobe; KIRC, Kidney Renal Clear Cell Carcinoma; KIRP, Kidney Renal Papillary Cell Carcinoma; LGG, Brain Lower Grade Glioma; LIHC, Liver Hepatocellular Carcinoma; LUAD, Lung Adenocarcinoma; LUSC, Lung Squamous Cell Carcinoma; MESO, Mesothelioma; OV, Ovarian Serous Cystadenocarcinoma; PAAD, Pancreatic Adenocarcinoma; PCPG, Pheochromocytoma and Paraganglioma; PRAD, Prostate Adenocarcinoma; READ, Rectum Adenocarcinoma; SARC, Sarcoma; SKCM, Skin Cutaneous Melanoma; STAD, Stomach Adenocarcinoma; TGCT, Testicular Germ Cell Tumors; THCA, Thyroid Carcinoma; THYM, Thymoma; UCEC, Uterine Corpus Endometrial Carcinoma; UCS, Uterine Carcinosarcoma; UVM, Uveal Melanoma.

(model no. CKX53, Olympus, Tokyo, Japan). The rate of wound closure was quantified by measuring the change in the wound area using ImageJ software (version 1.53, National Institutes of Health, Bethesda, MD, USA). The experiment was performed in triplicate.

2.14 Transwell Invasion and Migration Assays

Invasive and migratory abilities of A549 cells were tested using 24-well Transwell chambers with 8.0 µm pore size membranes (Corning, USA). In brief, cells were suspended in 200 µL of serum-free medium and placed in the upper chamber, while the lower chamber contained 500 µL of complete medium with 10% FBS as a chemoattractant. After 24 hours of incubation, non-invading/migrating cells on the upper surface of the membrane were removed with a cotton swab. Cells on the lower surface were fixed with 4% paraformaldehyde and stained with 0.1% crystal violet. The stained cells were imaged and counted in five randomly selected fields. Each assay was repeated three times.

2.15 Statistical Analysis

Statistical analyses were conducted using R software (version 4.0.2, R Foundation for Statistical Computing, Vienna, Austria), with a p-value < 0.05 indicating statistical significance. The Student's t-test was used for comparisons between two groups, and one-way ANOVA was applied for comparisons among multiple groups. To ensure the robustness of our differential expression results, adjustments for multiple testing were made. Furthermore, batch effects from the integrated TCGA and GEO datasets were corrected to enhance data consistency and accuracy.

3. Results

3.1 KIF18B Exhibits a Pattern of Overexpression Across Diverse Cancer Types

A systematic investigation of the TCGA and GTEx databases revealed a consistent pattern of *KIF18B* overexpression in most examined cancers when contrasted with healthy tissues (Fig. 1A,B; $p < 0.05$). This differential expression was also evident at the intra-patient level, where tumor tissues displayed significantly higher *KIF18B* transcript abundance than their corresponding adjacent normal tissues in paired analyses (Fig. 1C).

3.2 Diagnostic Value of KIF18B Expression in Differentiating Tumor From Normal Tissues

To assess the diagnostic value of *KIF18B*, we performed Receiver Operating Characteristic (ROC) analysis. The results confirmed that *KIF18B* expression has a strong capability to distinguish tumor from normal tissues across numerous cancer types. The AUC values were consistently high, reaching a peak of 0.976 in LUAD, which signifies excellent diagnostic accuracy. The smoothed ROC curves visually affirmed the robust discriminatory power of *KIF18B*, especially in several key malignancies (Fig. 2).

3.3 KIF18B Expression Serves as a Dual Prognostic Indicator in Cancer

Our investigation into the prognostic significance of *KIF18B* revealed a complex, context-dependent role. In a substantial number of malignancies, including LUAD, liver cancer (LIHC) and kidney clear cell carcinoma (KIRC), *KIF18B* acted as a significant risk factor. Patients within the high-*KIF18B* expression cohort demonstrated a markedly poorer Overall Survival (OS) compared to their low-expression counterparts (log-rank $p < 0.05$). Conversely, in a distinct subset of cancers, such as stomach cancer (STAD), elevated *KIF18B* levels were associated with a favorable prognosis and improved survival outcomes. These opposing survival patterns are clearly visualized in the Kaplan-Meier curves (Fig. 3), underscoring the dual prognostic nature of *KIF18B*.

3.4 High KIF18B Expression Corresponds to a Distinct Immune Phenotype

We next sought to characterize the immune phenotype associated with *KIF18B* expression. A comprehensive co-expression analysis revealed that *KIF18B* is tightly linked to a pro-inflammatory gene signature. The heatmap illustrates this trend, where *KIF18B* expression strongly covaries with genes central to T-cell activation and immune suppression across a majority of cancers (Fig. 4A). In parallel, when tumors were stratified into high- and low-*KIF18B* cohorts, we found a profound and statistically significant divergence in their immune subtype composition (chi-square test, $p < 0.001$). The C1 (Wound Healing) and C2 (IFN-gamma Dominant) subtypes were significantly overrepresented in the high-*KIF18B* group (Fig. 4B). Together, these analyses indicate that high *KIF18B* expression is a hallmark of an immunologically engaged but potentially exhausted tumor microenvironment.

To elucidate the functional consequences of elevated *KIF18B*, we analyzed differential pathway activity using proteomic data. This analysis revealed that *KIF18B*-high tumors were characterized by a significant upregulation of pathways central to cancer progression. Specifically, we observed a hyperactive state in pathways governing Epithelial-Mesenchymal Transition (EMT), Cell Cycle, and DNA Damage Response ($p < 0.05$) (Fig. 4C). These findings suggest that *KIF18B*'s prognostic impact may be mediated, at least in part, by its influence on these fundamental cellular processes.

The expression of *KIF18B* was found to be strongly correlated with the composition of the tumor immune microenvironment. As illustrated in the heatmap, *KIF18B* showed a predominantly positive association with the abundance of various immune cell populations across a wide spectrum of cancers (Fig. 4D). This was particularly prominent for immunosuppressive cells, such as regulatory T cells (Tregs), in cancers like LUAD. This suggests that

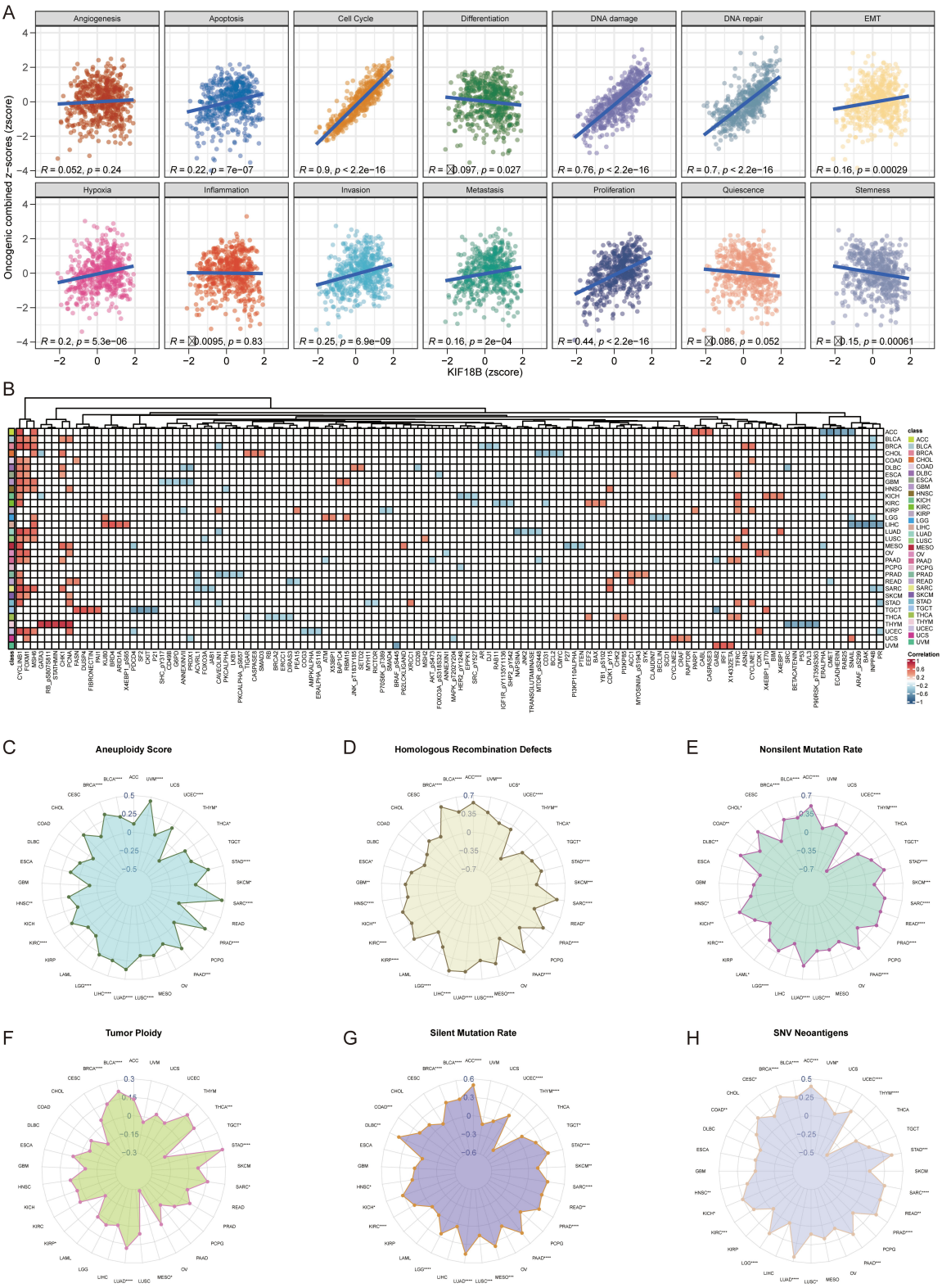

Fig. 5. Functional characterization and association of *KIF18B* with genomic instability. (A) Correlation analysis of *KIF18B* expression with the activity scores of 14 distinct cancer functional states, highlighting a strong positive association with Epithelial-Mesenchymal Transition (EMT), Cell Cycle, and DNA Damage. (B) Scatter plots showing the positive correlation of *KIF18B* with *CYCLINB1*, *FOXM1*, and *MSH6* in LUAD. (C–H) Radar chart visualizing the positive correlation between KIF18B expression and key genomic instability metrics, including Aneuploidy Score, Tumor Ploidy, and Nonsilent Mutation Rate, across pan-cancer.

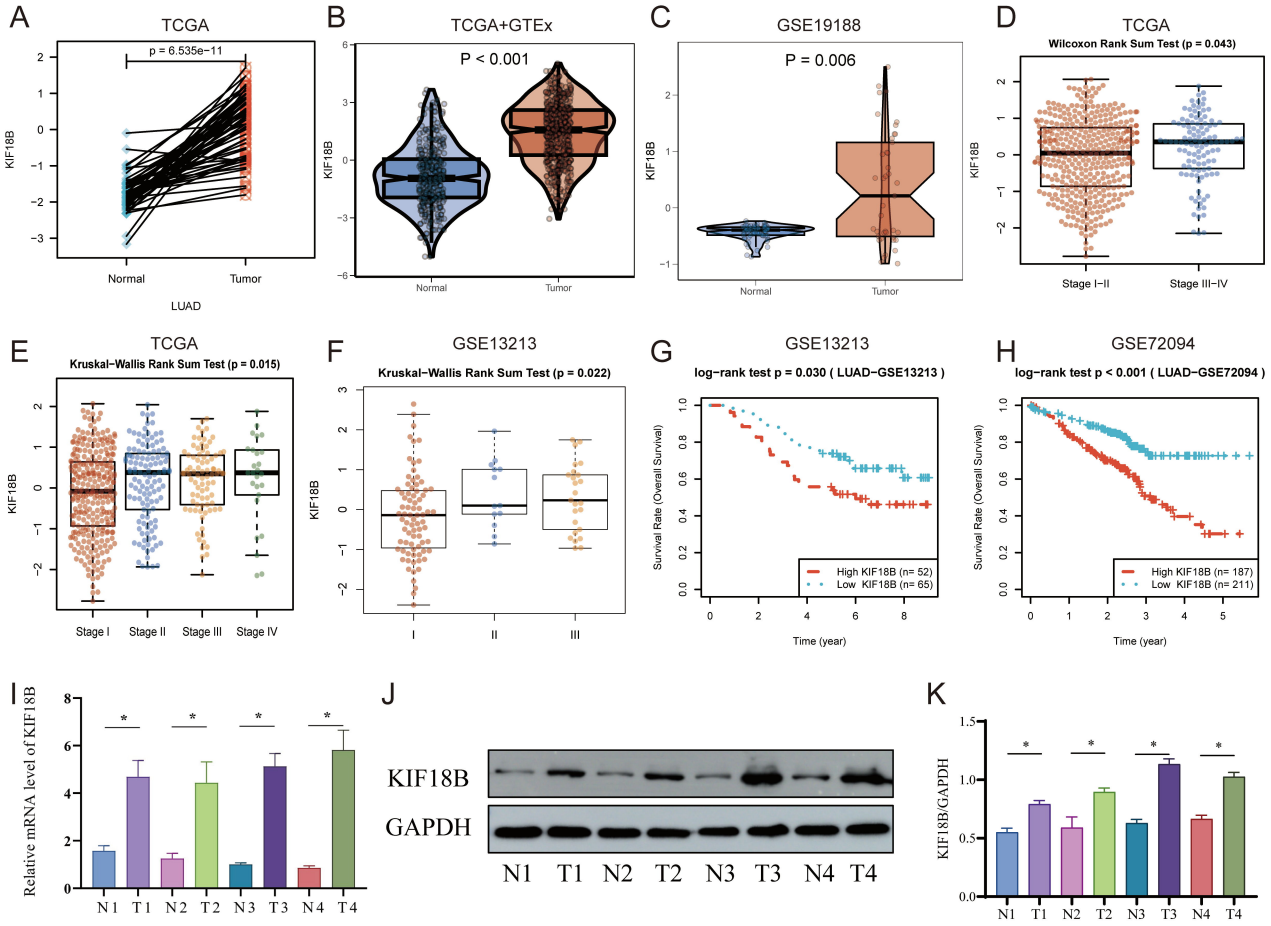

Fig. 6. Validation of KIF18B overexpression and its prognostic significance in lung adenocarcinoma (LUAD). (A,B) *KIF18B* expression is significantly upregulated in LUAD in the TCGA cohort ($p < 0.05$). (C) Validation of *KIF18B* upregulation in the GSE19188 dataset. (D,E) Box plots showing a positive correlation between *KIF18B* expression and advancing tumor stage in the TCGA-LUAD cohort. (F) Validation of the correlation between *KIF18B* and tumor grade in the GSE13213 dataset ($p < 0.05$). (G,H) Kaplan-Meier curves demonstrating that high *KIF18B* expression is associated with poorer overall survival in LUAD patients ($p < 0.05$). (I) RT-qPCR analysis showing elevated *KIF18B* mRNA levels in four pairs of LUAD compared to adjacent normal tissues. (J,K) Western blot analysis and corresponding quantification confirming the overexpression of KIF18B protein in LUAD tumor samples relative to matched adjacent tissues. *$p < 0.05$.

KIF18B may contribute to an immune-suppressive milieu, potentially facilitating tumor immune escape.

3.5 Functional Role and Pathway Analysis of KIF18B

To delineate the functional signature of *KIF18B*, we correlated its expression with the activity scores of 14 distinct cancer functional states. Our analysis uncovered a strong and consistent positive association between *KIF18B* levels and states related to EMT, Cell Cycle, and DNA Damage across multiple cancer types (Fig. 5A). This alignment suggests that *KIF18B* expression is intrinsically linked to the core cellular machinery that promotes tumor growth and progression, establishing it as a marker for a highly active and malignant phenotype. Fig. 5B indicates that in LUAD, *KIF18B* shows a strong positive correlation with *CYCLINB1*, *FOXM1*, and *MSH6*.

To investigate a potential link between *KIF18B* and genomic instability, we correlated its expression with several key genomic features. The resulting radar chart visualization shows a consistent positive association between high *KIF18B* expression and metrics of genomic disarray, including Aneuploidy Score, Tumor Ploidy, and Nonsilent Mutation Rate across pan-cancer (Fig. 5C–H). This pattern strongly suggests that *KIF18B* expression is a prominent feature of tumors characterized by a fundamentally unstable genome.

3.6 Differential Expression Level and Survival Analysis of KIF18B in LUAD

Within the TCGA-LUAD cohort, *KIF18B* expression was significantly upregulated in tumor samples compared to adjacent normal tissues ($p < 0.05$) (Fig. 6A,B). This

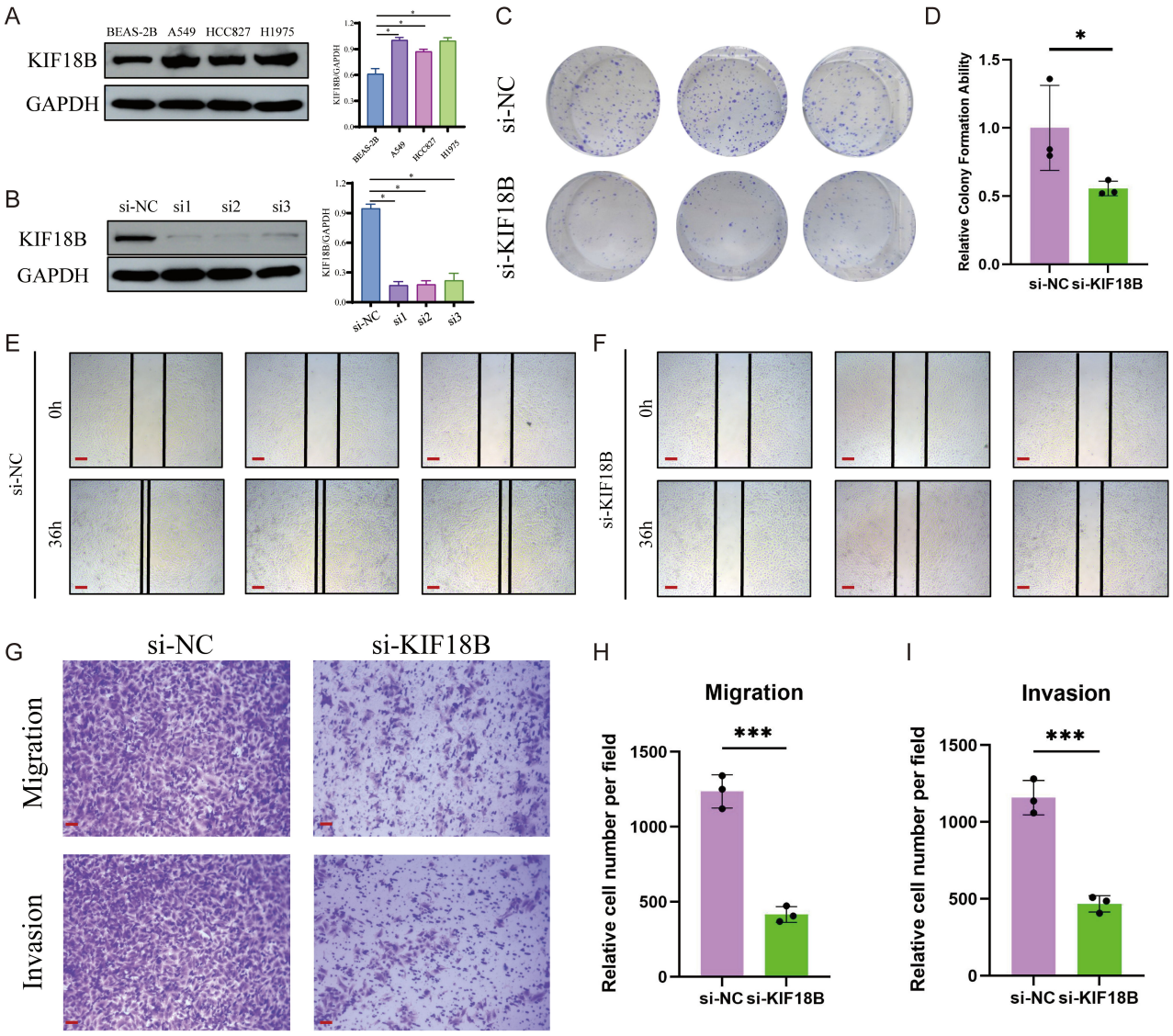

Fig. 7. Silencing of KIF18B impedes malignant phenotypes in LUAD cells *in vitro*. (A) Western blot analysis of endogenous KIF18B protein levels in human LUAD cell lines (A549, HCC827, H1975) and BEAS-2B. (B) Western blot confirming the effective knockdown of KIF18B in A549 cells by three different siRNAs. (C,D) Colony formation assay showing that KIF18B silencing reduces the proliferative capacity of A549 cells. (E,F) Wound healing assay demonstrating impaired migratory ability of A549 cells upon KIF18B knockdown. (G–I) Transwell assays showing a significant reduction in both migration and invasion capabilities of cells after KIF18B silencing. Representative images and quantification are shown. *$p < 0.05$, ***$p < 0.001$. Scale bars in (E,F): 250 µm. Scale bars in (G): 100 µm.

trend was validated in an independent dataset (GSE19188) (Fig. 6C). A graded analysis of *KIF18B* expression across different tumor stages revealed a clear trend of increased expression with higher tumor grade (Fig. 6D,E), a finding that was validated in an independent GEO dataset (GSE13213) ($p < 0.05$) (Fig. 6F). Furthermore, survival analysis indicated that higher *KIF18B* expression level was significantly associated with shorter overall survival in LUAD patients (Log-rank test, $p < 0.05$) (Fig. 6G,H).

3.7 Experimental Validation Confirms KIF18B Overexpression in LUAD Tissues

To experimentally validate the differential expression of KIF18B at both the mRNA and protein levels, we collected four pairs of LUAD and adjacent non-tumorous tissues. RT-qPCR analysis revealed that *KIF18B* mRNA levels were markedly upregulated in tumor relative to matched normal counterparts (Fig. 6I). Consistent with these transcriptomic findings, Western blot results demonstrated that KIF18B protein levels were also significantly elevated in the LUAD samples compared to the adjacent tissues

(Fig. 6J,K). Taken together, these results provide direct experimental evidence confirming that KIF18B is overexpressed in LUAD.

3.8 Effective Knockdown of KIF18B Expression by siRNA in A549 Cells

To establish a suitable *in vitro* model for functional studies, we first assessed the endogenous protein expression levels of KIF18B across a panel of human LUAD cell lines (A549, HCC827, H1975) and a normal human bronchial epithelial cell line (BEAS-2B). Western blot analysis revealed that KIF18B expression was notably upregulated in all cancer cell lines compared to the normal BEAS-2B cells. Among the tested cancer cell lines, A549 exhibited the highest abundance of endogenous KIF18B protein (Fig. 7A). Consequently, the A549 cell line was selected for all subsequent siRNA-mediated knockdown experiments.

Then, we employed small interfering RNAs (siRNAs) to specifically silence its expression in A549 cells. Three distinct siRNAs targeting *KIF18B* (si-KIF18B#1, #2, and #3) and a negative control (si-NC) were transfected into the cells. WB analysis demonstrated that all three si-KIF18B constructs significantly reduced KIF18B expression levels compared to the si-NC group. Notably, si-KIF18B#1 and si-KIF18B#2 exhibited the most potent silencing effects ($p < 0.01$, Fig. 7B). The silencing effect was also validated in the H1975 cell line (**Supplementary Fig. 1**).

3.9 Silencing KIF18B Attenuates Proliferation, Migration, and Invasion of A549 Cells

Following the successful knockdown of KIF18B in A549 cells, we investigated its impact on key malignant characteristics. The colony formation assay revealed that KIF18B depletion led to a significant reduction in both the number and size of cell colonies, indicating that KIF18B is required for long-term proliferative capacity ($p < 0.01$, Fig. 7C,D). Furthermore, the migratory ability of cells was markedly impaired upon KIF18B silencing. This was demonstrated by a significantly slower wound closure rate in the wound healing assay (Fig. 7E,F) and a dramatic decrease in the number of cells passing through the membrane in the Transwell migration assay (Fig. 7G). Consistent with these findings, the invasive potential of the cells was also substantially suppressed, as shown by the reduced cell count in the Transwell invasion assay ($p < 0.001$, Fig. 7G–I). Collectively, these results establish that KIF18B plays a pivotal role in promoting the proliferation, migration, and invasion of lung adenocarcinoma cells.

4. Discussion

Lung cancer remains the leading cause of cancer-related mortality worldwide, with lung adenocarcinoma (LUAD) being its most prevalent and insidious subtype [19–21]. Despite significant progress in targeted therapy and immunotherapy, the 5-year survival rate for LUAD patients remains disappointingly low, primarily due to acquired drug resistance and frequent tumor recurrence [22–24]. This grim clinical reality underscores an urgent and persistent need to identify novel molecular drivers that can serve as both reliable prognostic biomarkers and effective therapeutic targets to improve patient outcomes [25].

KIF18B is frequently over-expressed in a wide spectrum of malignancies—including cervical, breast, hepatocellular, and melanoma—where it drives tumor cell proliferation, migration, invasion and metastasis [26–29]. Mechanistically, *KIF18B* activates several oncogenic signaling cascades: it promotes Wnt/β-catenin signaling in cervical cancer [26]; it stimulates the PI3K/AKT-mTOR axis in prostate cancer cells [30]; and it enhances AKT/GSK-3β signaling that further reinforces β-catenin activity [27]. *KIF18B* also modulates microtubule dynamics and spindle positioning during mitosis, interacts with EB1 and γ-actin to regulate lysosome-associated mTORC1 signaling, and facilitates DNA double-strand break repair via 53BP1, thereby supporting cell cycle progression and survival [31]. Clinically, high *KIF18B* levels correlate with advanced tumor stage, poor overall survival and resistance to chemotherapy agents such as oxaliplatin in colorectal cancer [32], doxorubicin in breast cancer [27], and vincristine in diffuse large B-cell lymphoma [33]. It is important to note that our study suggests *KIF18B* exhibits a dual prognostic role across different types of cancer. It remains unclear whether the function of *KIF18B* is tumor type-specific or universally oncogenic, thus requiring further experimental evidence for confirmation in the future.

In this study, we identified Kinesin Family Member 18B (*KIF18B*), a motor protein classically known for its role in mitotic regulation, as a critical oncogene in human malignancies. Through a comprehensive approach integrating pan-cancer bioinformatic analysis with targeted experimental validation in LUAD, our findings robustly position *KIF18B* as a key player in tumor progression. Our pan-cancer analysis revealed a striking pattern of *KIF18B* overexpression across a wide spectrum of cancers, which strongly suggests its fundamental role in tumorigenesis. The exceptional diagnostic accuracy of *KIF18B*, particularly in LUAD (AUC = 0.976), highlights its potential as a powerful clinical biomarker for distinguishing malignant from healthy tissue.

Our study provides compelling mechanistic insights into how *KIF18B* drives malignancy. The classical function of *KIF18B* is to ensure chromosomal stability during mitosis. Our bioinformatic data suggest that its overexpression disrupts this delicate balance, as evidenced by the strong positive correlation between *KIF18B* expression and key hallmarks of genomic instability, including aneuploidy, tumor ploidy, and mutation rates. Furthermore, high *KIF18B* expression was strongly associated with the activation of pathways central to cancer progression, such as the cell cycle, DNA damage response, and epithelial-mesenchymal

transition (EMT). The observed co-expression with master regulators like *CYCLINB1* and *FOXM1* further implicates *KIF18B* as a core component of the cellular machinery that fuels relentless proliferation and invasion.

Crucially, our study did not rely solely on computational predictions. We proceeded to perform rigorous experimental validation, which serves as the cornerstone of our conclusions. We first confirmed the significant upregulation of *KIF18B* at both the mRNA and protein levels in clinical LUAD tissues and cell lines. Subsequently, by silencing KIF18B in A549 and H1975 cells, we directly demonstrated its functional necessity for maintaining malignant traits. The observed reduction in colony-forming ability and the stark impairment of migratory and invasive capacities upon KIF18B knockdown provide direct, tangible evidence of its oncogenic role. These *in vitro* results powerfully corroborate the functions predicted by our bioinformatic analyses, solidifying KIF18B's status as a driver of LUAD progression.

Despite the comprehensive scope of this research, several limitations must be acknowledged. First, the bioinformatic analyses, while powerful, are inherently correlational and do not definitively establish causality. Second, our experimental validation was primarily conducted in two LUAD cell lines (A549 and H1975), and further studies across a broader panel of cell lines with diverse genetic backgrounds are needed to ensure the generalizability of our findings. Third, while we have identified the phenotypic outcomes of KIF18B knockdown, the precise downstream molecular pathways require more in-depth investigation. Finally, this study lacks *in vivo* data. Future research using xenograft or genetically engineered mouse models will be essential to validate the role of *KIF18B* in tumor growth and metastasis within a complex physiological system.

5. Conclusion

In conclusion, our integrated study systematically characterizes *KIF18B* as a widely expressed pan-cancer oncogene with significant prognostic and diagnostic value. We provide strong experimental evidence that *KIF18B* is indispensable for the proliferation, migration, and invasion of LUAD cells. These findings collectively establish *KIF18B* not only as a promising biomarker for predicting patient outcomes but also as a compelling therapeutic target. However, while our results highlight the potential of *KIF18B* as a therapeutic target, further research, including pharmacologic inhibition studies and *in vivo* validation, is necessary to substantiate these claims.

Availability of Data and Materials

The public datasets analyzed in this study were sourced from their respective databases. The TCGA-LUAD cohort data were retrieved from The Cancer Genome Atlas (TCGA, https://xena.ucsc.edu/), while the GEO cohort data were acquired from the Gene Expression Omnibus (GEO, https://www.ncbi.nlm.nih.gov/gds/?term=). The datasets used and analyzed during the current study are available from the corresponding author on reasonable request.

Author Contributions

Conceptualization, XTX; Data curation, JLH and XRS; Methodology, WWX and YWZ; Software, WWX; Investigation, YWZ, WWX and FJ; Resources, XRS; Visualization, XRS and FJ; Writing – original draft, JLH; Writing – review & editing, XTX. Supervision, JLH; Project administration, XTX; Funding acquisition, XTX. All authors contributed to editorial changes in the manuscript. All authors read and approved the final manuscript. All authors have participated sufficiently in the work and agreed to be accountable for all aspects of the work.

Ethics Approval and Consent to Participate

This study was conducted in compliance with the Declaration of Helsinki and received ethical approval from the Institutional Review Board of The Affiliated Hospital of Yangzhou University (Approval Number: 2024-YKL07-SW007). Informed consent was obtained from all participating.

Acknowledgment

We would like to express our gratitude to all those who helped us during the writing of this manuscript. Thanks to all the peer reviewers for their opinions and suggestions.

Funding

This study was supported by 2024 Yangzhou Basic Research Program (Joint Special Projects) - Health and Wellness Category (No. 2024-03-15).

Conflict of Interest

The authors declare no conflict of interest.

Supplementary Material

Supplementary material associated with this article can be found, in the online version, at https://doi.org/10.31083/FBL47910.

References

[1] Siegel RL, Giaquinto AN, Jemal A. Cancer statistics, 2024. CA: a Cancer Journal for Clinicians. 2024; 74: 12–49. https://doi.org/10.3322/caac.21820.

[2] Scheepens JCC, Groenvold M, Giesinger JM, Dirven L, Thurner AMM, Bjelic-Radisic V, *et al*. The use of EORTC QLQ-C30 Summary Score in cancer research and its performance as compared with the EORTC QLQ-C30 Global Health/Quality of Life scale: A systematic review and comparative analysis of effect sizes. European Journal of Cancer (Oxford, England: 1990). 2025; 231: 116064. https://doi.org/10.1016/j.ejca.2025.116064.

[3] Nematzadeh S, Karaul A. Advances in Computational Drug Repurposing, Driver Genes, and Therapeutics in Lung Adenocar-

cinoma. Biomolecules. 2025; 15: 1373. https://doi.org/10.3390/biom15101373.

[4] Wang Y, Xu M, Wei X, Huang H, Chen Q, Chen B, *et al*. Prospective proteomics for discovering biomarkers in lung adenocarcinoma: a literature review. Translational Cancer Research. 2025; 14: 6102–6117. https://doi.org/10.21037/tcr-2025-1092.

[5] Ceccarelli I, Durand M, Seguin-Givelet A. The evolving role of wedge resection in early-stage non-small cell lung cancer: a literature review. Translational Lung Cancer Research. 2025; 14: 4078–4094. https://doi.org/10.21037/tlcr-2025-562.

[6] Otis SU, Banna GL, Maniam A. Perioperative Immunotherapy for Non-Small Cell Lung Cancer (NSCLC). Current Oncology Reports. 2025; 27: 1358–1373. https://doi.org/10.1007/s11912-025-01720-z.

[7] Galera P, Iglesias-Beiroa A, Hernández-Marín B, Bañón D, Arangoa T, Castillo L, *et al*. Chemokine Receptors in Peripheral Blood Mononuclear Cells as Predictive Biomarkers for Immunotherapy Efficacy in Non-Small Cell Lung Cancer. Current Oncology (Toronto, Ont.). 2025; 32: 583. https://doi.org/10.3390/curroncol32100583.

[8] Wang Y, Zhang L, Zhao X, Sun D, Zhou H, Zhang Y, *et al*. Efficacy and safety of perioperative, adjuvant and neoadjuvant chemoimmunotherapy stratified by clinical stage and PD-L1 expression in resectable non-small cell lung cancer: a systematic review and network meta-analysis. Translational Lung Cancer Research. 2025; 14: 3378–3395. https://doi.org/10.21037/tlcr-2025-426.

[9] Liu S, Chen J, Shi L, Deng Y, Wang Z. Research progress of kinesin family in neurological diseases. Frontiers in Cellular Neuroscience. 2025; 19: 1527305. https://doi.org/10.3389/fncel.2025.1527305.

[10] Shagufta, Aftab M, Sisodiya S, Mishra S, Priya K, Hussain S. Prognostic significance of the kinesin superfamily in breast cancer: A systematic review & meta-analysis. The Indian Journal of Medical Research. 2025; 161: 627–635. https://doi.org/10.25259/IJMR_2072_2024.

[11] Ghnim ZS, Mahdi MS, Ballal S, Chahar M, Verma R, Al-Nuaimi AMA, *et al*. The role of kinesin superfamily proteins in hepatocellular carcinoma. Medical Oncology (Northwood, London, England). 2024; 41: 271. https://doi.org/10.1007/s12032-024-02497-0.

[12] McHugh T, Welburn JPI. Potent microtubule-depolymerizing activity of a mitotic Kif18b-MCAK-EB network. Journal of Cell Science. 2023; 136: jcs260144. https://doi.org/10.1242/jcs.260144.

[13] Stout JR, Yount AL, Powers JA, Leblanc C, Ems-McClung SC, Walczak CE. Kif18B interacts with EB1 and controls astral microtubule length during mitosis. Molecular Biology of the Cell. 2011; 22: 3070–3080. https://doi.org/10.1091/mbc.E11-04-0363.

[14] Huang T, Zhang J. Therapeutic Suppression of Triple-Negative Breast Cancer via Pachymic Acid-Induced KIF18B Inhibition and Ferroptosis Activation. Molecular Carcinogenesis. 2025; 64: 2075–2085. https://doi.org/10.1002/mc.70045.

[15] Saadh MJ, Ghnim ZS, Mahdi MS, Mandaliya V, Ballal S, Bareja L, *et al*. The emerging role of kinesin superfamily proteins in Wnt/β-catenin signaling: Implications for cancer. Pathology, Research and Practice. 2025; 269: 155904. https://doi.org/10.1016/j.prp.2025.155904.

[16] Thorsson V, Gibbs DL, Brown SD, Wolf D, Bortone DS, Ou Yang TH, *et al*. The Immune Landscape of Cancer. Immunity. 2018; 48: 812–830.e14. https://doi.org/10.1016/j.immuni.2018.03.023.

[17] Lee E, Chuang HY, Kim JW, Ideker T, Lee D. Inferring pathway activity toward precise disease classification. PLoS Computational Biology. 2008; 4: e1000217. https://doi.org/10.1371/journal.pcbi.1000217.

[18] Sun D, Wang J, Han Y, Dong X, Ge J, Zheng R, *et al*. TISCH: a comprehensive web resource enabling interactive single-cell transcriptome visualization of tumor microenvironment. Nucleic Acids Research. 2021; 49: D1420–D1430. https://doi.org/10.1093/nar/gkaa1020.

[19] Sun Y, Xu L, Deng C, Du X, Yu Y, Hao Y, *et al*. Distinct survival, optimal combination strategy of immunotherapy, and immunophenotype in uncommon and 20ins EGFR-mut lung adenocarcinoma: a multi-center study. Molecular Biomedicine. 2025; 6: 88. https://doi.org/10.1186/s43556-025-00331-1.

[20] Xie L, Zhou Y, Hu Z, Zhang W, Zhang X. Integrative multi-omics reveals energy metabolism-related prognostic signatures and immunogenetic landscapes in lung adenocarcinoma. Frontiers in Immunology. 2025; 16: 1679464. https://doi.org/10.3389/fimmu.2025.1679464.

[21] Wu S, Pan J, Zheng Y, Pan Q, Tan Y. Integration of Machine Learning, Bioinformatics, and Experimental Validation to Identify Novel Diagnostic and Prognostic Biomarkers Associated With Succinylation in Lung Adenocarcinoma. Drug Development Research. 2025; 86: e70184. https://doi.org/10.1002/ddr.70184.

[22] Zhang X, Wen Y, Wu F, Jiang Y, Lin Y, Wang L, *et al*. GSTA1 Conferred Tolerance to Osimertinib and Provided Strategies to Overcome Drug-Tolerant Persister in EGFR-Mutant Lung Adenocarcinoma. Journal of Thoracic Oncology: Official Publication of the International Association for the Study of Lung Cancer. 2025. https://doi.org/10.1016/j.jtho.2025.10.001. (in press)

[23] Chen M, Jiang W, Zhan J, Zhang S, Zheng J, Huang Y, *et al*. Activating NEDD4L suppresses EGFR-driven lung adenocarcinoma growth via facilitating EGFR proteasomal degradation. Journal of Experimental & Clinical Cancer Research: CR. 2025; 44: 294. https://doi.org/10.1186/s13046-025-03528-y.

[24] Du J, Zheng B, Qian J, Huang G, Yuan W, Huang R, *et al*. Hypoxia-induced exosomal LUCAT1 promotes osimertinib resistance in lung adenocarcinoma by stabilizing c-MET. Cell Death & Disease. 2025; 16: 763. https://doi.org/10.1038/s41419-025-08100-2.

[25] Banerjee A, Vathiotis I, Halder D, Sen U, Wang X, Shields MD, *et al*. Molecular Landscape and Therapeutic Strategies of Lung Cancer Lineage Plasticity. Journal of Thoracic Oncology: Official Publication of the International Association for the Study of Lung Cancer. 2025; 20: 1582–1593. https://doi.org/10.1016/j.jtho.2025.06.012.

[26] Wu Y, Wang A, Zhu B, Huang J, Lu E, Xu H, *et al*. KIF18B promotes tumor progression through activating the Wnt/β-catenin pathway in cervical cancer. OncoTargets and Therapy. 2018; 11: 1707–1720. https://doi.org/10.2147/OTT.S157440.

[27] Jiang J, Liu T, He X, Ma W, Wang J, Zhou Q, *et al*. Silencing of KIF18B restricts proliferation and invasion and enhances the chemosensitivity of breast cancer via modulating Akt/GSK-3β/β-catenin pathway. BioFactors (Oxford, England). 2021; 47: 754–767. https://doi.org/10.1002/biof.1757.

[28] Li Q, Sun M, Meng Y, Feng M, Wang M, Chang C, *et al*. Kinesin family member 18B activates mTORC1 signaling via actin gamma 1 to promote the recurrence of human hepatocellular carcinoma. Oncogenesis. 2023; 12: 54. https://doi.org/10.1038/s41389-023-00499-7.

[29] Yan H, Zhu C, Zhang L. Kinesin family member 18B: A contributor and facilitator in the proliferation and metastasis of cutaneous melanoma. Journal of Biochemical and Molecular Toxicology. 2019; 33: e22409. https://doi.org/10.1002/jbt.22409.

[30] Wu YP, Ke ZB, Zheng WC, Chen YH, Zhu JM, Lin F, *et al*. Kinesin family member 18B regulates the proliferation and invasion of human prostate cancer cells. Cell Death & Disease.

2021; 12: 302. https://doi.org/10.1038/s41419-021-03582-2.
[31] Chen S, Yu B, DU GT, Huang TY, Zhang N, Fu N. KIF18B: an important role in signaling pathways and a potential resistant target in tumor development. Discover Oncology. 2024; 15: 430. https://doi.org/10.1007/s12672-024-01330-4.
[32] Hong B, Lu R, Lou W, Bao Y, Qiao L, Hu Y, *et al*. KIF18b-dependent hypomethylation of PARPBP gene promoter enhances oxaliplatin resistance in colorectal cancer. Experimental Cell Research. 2021; 407: 112827. https://doi.org/10.1016/j.yexcr.2021.112827.
[33] Rovsing AB, Thomsen EA, Nielsen I, Skov TW, Luo Y, Dybkaer K, *et al*. Resistance to vincristine in DLBCL by disruption of p53-induced cell cycle arrest and apoptosis mediated by KIF18B and USP28. British Journal of Haematology. 2023; 202: 825–839. https://doi.org/10.1111/bjh.18872.